Finite size effects in surface emitting Terahertz quantum cascade lasers

Lukas Mahler,[1,*] Alessandro Tredicucci,[1] Fabio Beltram,[1] Christoph Walther,[2] Harvey E. Beere,[3] and David A. Ritchie[3]

[1] *NEST CNR-INFM, Scuola Normale Superiore, Piazza dei Cavalieri 7, I-56126, Pisa, Italy*
[2] *Institute for Quantum Electronics, ETH Zurich, HPT H 7, Wolfgang-Pauli-Str. 16, CH- 8093 Zurich, Switzerland*
[3] *Cavendish Laboratory, University of Cambridge, J J Thomson Avenue, Cambridge CB3 0HE, United Kingdom*
[*] *Corresponding author: l.mahler@sns.it*

Abstract: We analyze surface-emitting distributed feedback resonators for Terahertz quantum cascade lasers fabricated from double-metal waveguides. We explain the influence on resonances and surface-emission properties of the finite length and width of the gratings in connection with absorbing boundary conditions, and show that, contrary to the infinite case, the modes on either side of the photonic band-gap have finite surface losses. The lateral design of the resonator is shown to be important to avoid transverse modes of higher order and anti-guiding effects. Experimental findings are indeed in excellent agreement with the simulations. Both modeling and fabrication can easily be applied to arbitrary gratings, of which we discuss here a first interesting example.

OCIS codes: (140.3070) Infrared and far-infrared lasers; (140.3490) Lasers, distributed-feedback; (140.5965) Semiconductor lasers, quantum cascade; (240.6680) Surface plasmons; (250.7270) Vertical emitting lasers.

References and links

1. R. Köhler, A. Tredicucci, F. Beltram, H. E. Beere, E. H. Linfield, A. G. Davies, D. A. Ritchie, R. C. Iotti, and F. Rossi, "Terahertz semiconductor-heterostructure laser," Nature **417**, 156-159 (2002).
2. B. S. Williams, "Terahertz quantum-cascade lasers," Nature Photonics **1**, 517-525 (2007).
3. H.-W. Hübers, S. G. Pavlov, H. Richter, A. D. Semenov, L. Mahler, A. Tredicucci, H. E. Beere, and D. A. Ritchie, "High-resolution gas phase spectroscopy with a distributed feedback terahertz quantum cascade laser," Appl. Phys. Lett. **89**, 061115 (2006).
4. A. W. M. Lee, Q. Qin, S. Kumar, B. S. Williams, and Q. Hu "Real-time terahertz imaging over a standoff distance (>25 meters)," Appl. Phys. Lett. **89**, 141125 (2006).
5. S. Kumar and A. W. M. Lee "Resonant-phonon terahertz quantum-cascade lasers and video-rate terahertz imaging," IEEE J. Sel. Top. Quantum Electron. **14**, 333-344 (2008).
6. H.-W. Hübers, S. Pavlov, A. Semenov, R. Köhler, L. Mahler, A. Tredicucci, H. Beere, D. Ritchie, and E. Linfield, "Terahertz quantum cascade laser as local oscillator in a heterodyne receiver," Opt. Express **13**, 5890-5896 (2005).
7. B. S. Williams, S. Kumar, H. Callebaut, Q. Hu, and J. L. Reno "Terahertz quantum-cascade laser at $\lambda \approx 100$ µm using metal waveguide for mode confinement," Appl. Phys. Lett. **83**, 2124-2126 (2003).
8. B. S. Williams, S. Kumar, Q. Hu, and J. Reno, "Operation of terahertz quantum-cascade lasers at 164 K in pulsed mode and at 117 K in continuous-wave mode," Opt. Express **13**, 3331-3339 (2005).
9. M. A. Belkin, J. A. Fan, S. Hormoz, F. Capasso, S. P. Khanna, M. Lachab, A. G. Davies, and E. H. Linfield, "Terahertz quantum cascade lasers with copper metal-metal waveguides operating up to 178 K," Opt. Express **16**, 3242-3248 (2008).
10. M. I. Amanti, M. Fischer, C. Walther, G. Scalari, J. Faist, "Horn antennas for terahertz quantum cascade lasers," Electron. Lett. **43**, 573-574, (2007).
11. W. Maineult, P. Gellie, A. Andronico, P. Filloux, G. Leo, C. Sirtori, S. Barbieri, E. Peytavit, T. Akalin, J.-F. Lampin, H. E. Beere, and D. A. Ritchie, "Metal-metal terahertz quantum cascade laser with micro-transverse-electromagnetic-horn antenna," Appl. Phys. Lett. **93** 183508 (2008).
12. A. W. M. Lee, Q. Qin, S. Kumar, B. S. Williams, Q. Hu, and J. L. Reno, "High-power and high-temperature THz quantum-cascade lasers based on lens-coupled metal-metal waveguides," Opt. Lett. **32**, 2840-2842, (2007).

#106771 - $15.00 USD Received 23 Jan 2009; revised 26 Mar 2009; accepted 5 Apr 2009; published 8 Apr 2009

13. O. Demichel, L. Mahler, T. Losco, C. Mauro, R. Green, A. Tredicucci, J. Xu, F. Beltram, H. E. Beere, D. A. Ritchie, and V. Tamošinuas, "Surface plasmon photonic structures in terahertz quantum cascade lasers," Opt. Express **14**, 5335-5345 (2006).
14. J. A. Fan, M. A. Belkin, F. Capasso, S. Khanna, M. Lachab, A. G. Davies, and E. H. Linfield, "Surface emitting terahertz quantum cascade laser with a double-metal waveguide," Opt. Express **14**, 11672-11680 (2006).
15. S. Kumar, B. S. Williams, Q. Qin, A. W. Lee, Q. Hu, and J. L. Reno, "Surface-emitting distributed feedback terahertz quantum-cascade lasers in metal-metal waveguides," Opt. Express **15**, 113-128 (2007).
16. C. Pflügl, M. Austerer, W. Schrenk, S. Golka, G. Strasser, R. P. Green, L. R. Wilson, J. W. Cockburn, A. B. Krysa, and J. S. Roberts, "Single-mode surface-emitting quantum-cascade lasers," Appl. Phys. Lett. **86** 211102 (2005).
17. M. Schubert and F. Rana, "Analysis of Terahertz Surface Emitting Quantum-Cascade Lasers," IEEE J. Quantum Electron. **42**, 257 (2006).
18. M. A. Ordal, R. J. Bell, R. W. Alexander, Jr., L. L. Long, and M. R. Querry, "Optical properties of Au, Ni, and Pb at submillimeter wavelengths," Appl. Opt. **26**, 744 (1987).
19. L. Mahler, A. Tredicucci, F. Beltram, C. Walther, J. Faist, B. Witzigmann, H. E. Beere, and D. A. Ritchie "Vertically emitting microdisk lasers," Nat. Photonics **3**, 46 - 49 (2009).
20. L. Mahler, A. Tredicucci, R. Köhler, F. Beltram, H.E. Beere, E.H. Linfield, and D.A. Ritchie "High-Performance operation of single-mode terahertz quantum cascade lasers with metallic gratings," Appl. Phys. Lett. , **87**, 181101 (2004).
21. J. A. Fan, M. A. Belkin, F. Capasso, S. P. Khanna, M. Lachab, A. Giles Davies, and Edmund H. Linfield "Wide-ridge metal-metal terahertz quantum cascade lasers with high-order lateral mode suppression," Appl. Phys. Lett. **92** 031106 (2008).

1. Introduction

Terahertz quantum cascade lasers (THz QCLs) were first demonstrated in 2002 [1] and have since undergone rapid development [2]. They are investigated as potential sources in spectroscopy [3], imaging [4,5] and heterodyne systems [6]. Their waveguides are based on surface plasmons, either in single-metal [1], or double-metal configuration [7]. In the latter case, the waveguide consists of the gain material sandwiched between two metallic layers. The two surface-plasmons at the metal-dieletric interfaces form a mode of transverse-magnetic (TM) nature, which ideally matches the selection rules of intersubband transitions. Such a waveguide has a confinement factor close to unity, while keeping the losses moderate, and has been shown to perform significantly better than the single-metal waveguide at higher operating temperatures [8,9]. From an application point of view, however, Fabry-Perot resonators based on these subwavelength waveguides, due to the strong impedance mismatch at the facet and an intrinsically strong divergence of the beam, make it difficult to achieve high radiative and collection efficiencies. The integration into standard optical setups is thus often problematic. One of the most active fields of research for THz QCLs is therefore focusing on the improvement of the emission far-field pattern, either through horn antennas [10,11], hyperhemispherical silicon lenses [12], or gratings for vertical emission [13-15]. For the latter case, the waveguide is perturbed with a periodicity corresponding to the guided wavelength, which creates a distributed feedback (DFB) resonator, leading to emission in a single spectral mode. Additionally, in these so-called second order gratings, each perturbation acts as a radiation source and a good far-field profile in the vertical direction is obtained by constructive interference, similar to a phased-array device [16]. For metal-metal THz QCLs, this concept has first been theoretically investigated by Schubert et al., who discussed lasing thresholds, radiative efficiencies and far-fields of infinitely wide gratings [17]. Devices of finite length were considered by introducing highly reflecting metal facets at appropriate positions, in order to optimize the above properties. In the absence of such boundaries, the laser would always oscillate on the lower threshold mode whose symmetry with respect to the grating forbids vertical out-coupling. While the work offered many insights into the design of the grating, it did not address the lateral design of the resonator. A subsequent report on the experimental realization showed the importance of this issue, as many higher-order transverse

#106771 - $15.00 USD Received 23 Jan 2009; revised 26 Mar 2009; accepted 5 Apr 2009; published 8 Apr 2009

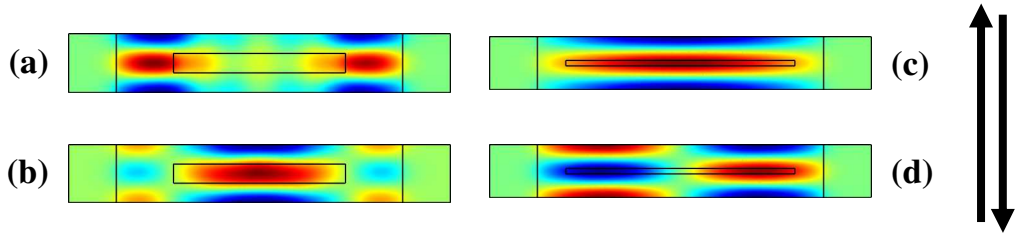

Fig. 1. Three dimensional modeling of the laser ridge. Only one unit cell of the grating is considered, and a top view of the electric field distribution of the eigenmodes is plotted. The propagation direction is indicated by the arrow. a), b) Lowest loss modes of a design taken from [14], c),d) lowest loss modes of the design in this work.

modes were observed in preliminary devices, which were explained by a three dimensional finite element model [15]. The same work reported a second device generation with a SiO_2/gold stack on all sides of the resonator, for the implementation of highly reflecting end facets, and, at the same time, to introduce losses for higher order transverse modes. While this resonator is well suited for a THz QCL, it is challenging in terms of design and fabrication, and the relatively narrow waveguide (~λ/2) leads to a considerable far-field divergence perpendicular to the grating. A similar device with a wider waveguide and an easier fabrication procedure was reported in an earlier work by Fan et al. [14], who used absorbers instead of highly reflecting boundaries. Following the arguments given in [17], however, of the two eigenmodes of the grating, only the one with zero vertical out-coupling should be excited in this case, owing to its much lower losses; the origin of the vertical out-coupling mechanism remained then somewhat unclear. Furthermore, the lateral mode distribution was not considered. This is the starting point of the present work, where we first give guidelines on when a two dimensional model like in [17] is justified, and generalize it to a model of the full longitudinal device design. This indeed allows us to explain the surface emission observed in devices with longitudinal absorbers. In addition, by comparison of the predicted spectral and spatial emission properties with those of a newly fabricated device, we demonstrate the predictive power of the model.

The work presented here identifies the aspects which have to be taken into account in the design of finite-size gratings, thus providing a framework allowing the computational characterization of arbitrary grating designs, In many possible applications, for instance, better surface emission properties could very likely be obtained with a non-periodic grating. We believe our approach to be an ideal tool to look for structures optimized not only in terms of spectral and spatial emission, but also in terms of coupling efficiency and overlap of optical mode and gain medium. As a preliminary example, we suggest the introduction of phase-shifts into a periodic grating in order to increase the surface losses of the device.

2. Transverse design

In order to understand the issues related to a finite-width grating, we consider the three dimensional unit cell of an infinitely long device. All the following differential equations were solved with a commercial finite element solver (Comsol Multiphysics). The high computational load of a three dimensional simulation including very thin metal and contact layers is avoided in the following way: We start with a 1D mode-analysis of a slab waveguide formed by active region, gold-, and contact-layers, with n_{het}=3.55-0.005i, n_{gold} taken from [18], and $n_{contact}$ computed with a Drude model. The imaginary part of the refractive index is a rough estimate, because the influence of electronic subband states on the losses is a complicated issue. An effective refractive index of 3.6-0.01i is obtained. We then sandwich a cuboid with this refractive index between perfect electric conductors of appropriate shape, and apply periodic boundary conditions. Two different designs are considered; Fig. 1 reports a top view of the two lowest-loss modes of each design. The first design is the one used in [14],

#106771 - $15.00 USD Received 23 Jan 2009; revised 26 Mar 2009; accepted 5 Apr 2009; published 8 Apr 2009

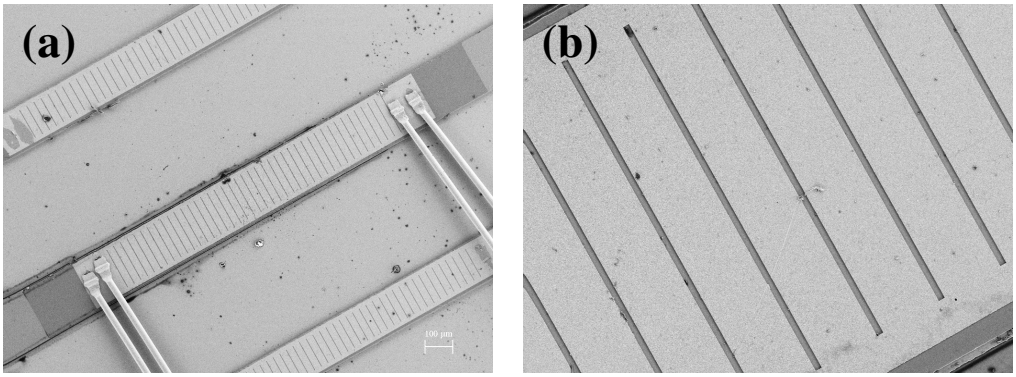

Fig. 2. (a). Top view of a fabricated device, the dark grey at the end of the grating metallization are the Cr pads that act as end absorbers. (b). Enlarged view of the grating, the slits are kept narrow, in order to maintain uniform pumping, and extend over a large part of the waveguide to avoid anti-guiding effects. One period is 27.3 μm.

while the second is the one we employed for the experiments in this work. In both cases, the waveguide is 150 μm wide, but while in the first grating the slit is 90 μm wide, in the second, it is 120 μm wide, and the grating duty cycle (dc) is 0.65 and 0.9, respectively. The periods are chosen at 29.8 μm and 27.3 μm to have the resonances within the gain of the employed active regions. Comparing the computed eigenfrequencies of the first case (2.900 THz and 3.036 THz) with the emission reported in [14] (2.865 THz), we conclude that the laser showed in that work oscillated on the mode with the electric field maxima under the side metallization. The existence of this mode can be explained with an anti-guiding effect: The effective refractive index n_{eff} of a double-metal structure (~3.6) is larger than n_{eff} of the open structure (~2.7) that forms the slit. The large slits in the center of the waveguide thus create a zone with a smaller average refractive index, and the photons are guided by the side metallization. Consequently, this effect is stronger for a larger side metallization and a small duty-cycle. The second mode is reminiscent of the original waveguide mode, but its excitation is less likely, also because the pumping is hampered due to the large opening in the electrical contact. In contrast, the second design with its high duty cycle and narrow side metallization avoids these problems, and the two lowest loss modes have the usual field distribution of a broad metallic waveguide. Apart from the improved pumping, engineering of the laser to oscillate on a wide mode like the one of Fig. 1(c) is important to obtain the best possible far-field perpendicular to the ridge.

3. Finite length analysis

The design described above allows the application of a significantly simpler model for the resonator analysis: the waveguide can be cut in the center along the propagation axis, and the eigenfrequencies in the plane given by propagation and growth axis can be computed. Translational invariance in the third dimension is assumed (infinitely wide grating). Since this reduces the computational domain to two dimensions, and simplifies the eigenfrequency equation to a scalar problem,

$$\nabla \cdot \left(\frac{1}{n^2(x,y)} \nabla H_z\right) = \frac{\omega^2}{c^2} H_z$$

(H_z is the magnetic field component perpendicular to the plane) it is possible to consider the full length of the device consisting of 42 periods plus 200 um long absorbers on each end, and take into account all thin gold and contact layers with their complex refractive indices as for the slab analysis above. Figure 2 shows a device, fabricated from the same wafer as [19]. Prior

#106771 - $15.00 USD Received 23 Jan 2009; revised 26 Mar 2009; accepted 5 Apr 2009; published 8 Apr 2009

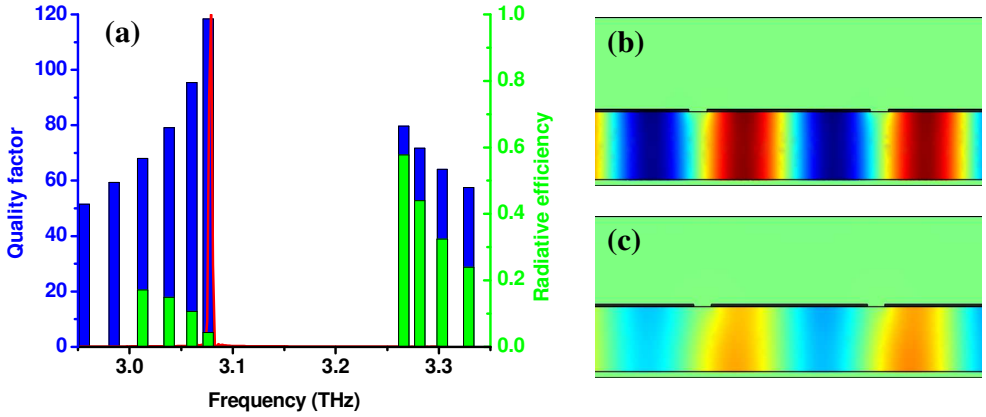

Fig. 3. (a). Computed (columns) and measured (red line) spectra of the device with a period of 27.3 μm and a grating duty-cycle of 90 % , depicted in Fig. 2. The computed spectrum is obtained by a two dimensional eigenfrequency analysis. The height of the green bars indicates the radiative efficiency and that of the blue ones the value of the quality factor. The right panel shows the magnetic field of the computed eigenmode corresponding to the lasing resonance in panel a), at the center of the resonator (b), and at the end of the resonator (c). The small shift in the mode with respect to the grating at the end leads to the surface emission.

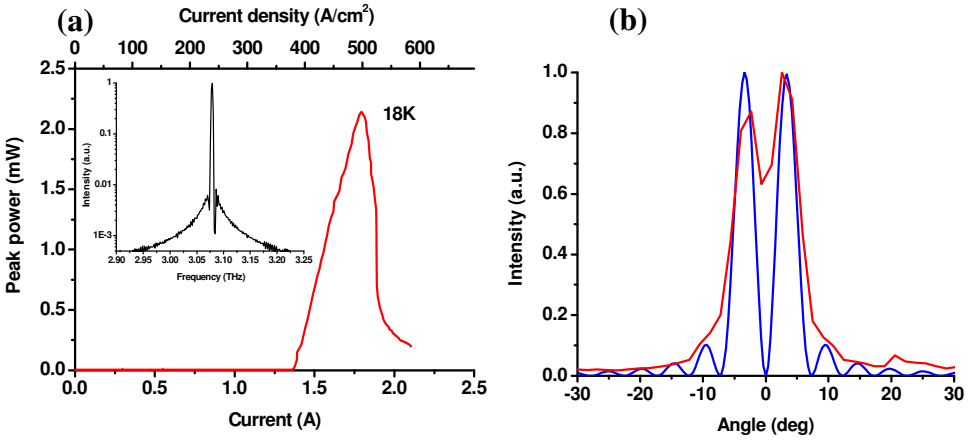

Fig. 4. (a). Vertically emitted peak power vs. current of a device operated with 800 ns pulses at 50 kHz repetition rate. No collection optics is employed, and the values are not corrected for the cryostat window. For the current density, the device area was assumed to be 200x1800 μm. (extension of the metallization). The inset shows the measured spectrum on a logarithmic scale. A side-mode suppression ratio of more than 20 dB is observed. (b). Far-field pattern of the device. The blue and red line show computed and measured far-field, respectively. The angle is measured with respect to the surface normal of the device, in the plane formed by surface normal and waveguide direction.

to grating fabrication, a thin Cr border is fabricated, masking the highly doped contact layer while the latter is removed in the slits, which creates an efficient absorber, both along and at the end of the grating. Devices similar to [14] are obtained, except for the slit design. The absorber on the waveguide edges is fabricated in order to keep the device single mode by introducing higher losses to the mode shown in Fig. 1(d), in analogy to [20, 21]. Figure 3(a) shows the computed spectrum (blue columns). The resonance with the highest quality factor

#106771 - $15.00 USD Received 23 Jan 2009; revised 26 Mar 2009; accepted 5 Apr 2009; published 8 Apr 2009

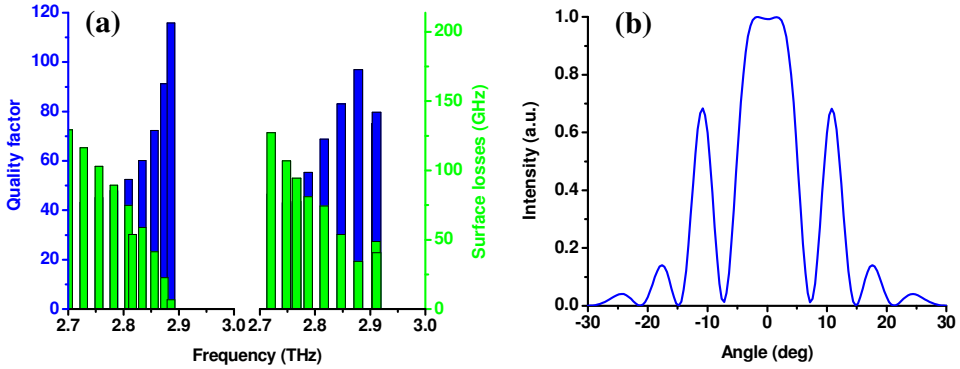

Fig. 5. (a). Comparison between a standard and a modified grating, each with a period of 30 μm and a grating duty-cycle of 80 %. Left and right panel show a standard and a modified grating respectively. By introducing two small phase-shifts, the surface losses can be increased by a factor of 5, while maintaining a favorable spectrum. Resonances above the photonic band-gap are not plotted, as they have low quality factors. (b). Computed far-field of the highest quality factor mode of the modified grating.

at 3.076 THz not only corresponds very well to the measured emission (red line), but also to the frequency of the mode shown in Fig. 1(c) (3.078 THz), justifying the simplification of an infinitely wide grating. The modes at the band-edges have the highest Q; because of their single-lobe spatial mode-distribution along the device, they have the smallest overlap with the absorbing end pads. The green columns show the radiative efficiency of each mode, which is the ratio between normalized surface losses and inverse photon lifetime. Unlike in the case of an infinitely long grating, the anti-symmetric mode at the lower band-edge has finite surface losses, which is easily understood in a model of the full device length. Figures 3(b), 3(c) show sections of the magnetic field in the center of the device, and towards the end of the grating. The finite length leads to a small chirp of the magnetic field with respect to the grating, and, therefore, removes the anti-symmetry (as observed in the center of the device or in an infinitely long grating), so that the positive and negative components of the magnetic field no longer interfere destructively, which in turn leads to surface emission. Note that we compute zero surface emission for the cases of Figs. 1(a, 1c), which indicates that the finite lateral size of the mode does not contribute to the out-coupling, and consequently, the quality factors and radiative efficiencies of the real device should be accurately described by a two dimensional model.

Figure 4(a) shows peak power vs. current of the device of Fig. 3(a) operating on the lower band-edge; it was measured with a Golay-cell ~3 cm above the device without any optics, and not corrected for the cryostat window. The slope efficiency of 5mW/A is rather modest in comparison with [15], where up to 40mW/A was obtained, owing to the optimized out-coupling and collection efficiency. The slope efficiency is here also reduced because the grating resonance at 3.08 THz is considerably detuned from the gain, which typically peaks at 3.12-3.3 THz as can be observed from the laser emission in Fabry-Perot resonators. The inset of Fig. 4(a) shows a spectrum on a logarithmic scale. Despite the detuning, we obtain a side-mode suppression ratio of more than 20 dB, which demonstrates the good selectivity of the grating. The strongest evidence of the good agreement between modeling and experiment can be obtained by considering the far-fields. We measured the angular intensity distribution in the plane spanned by propagation- and vertical device-axis by rotating the laser, while keeping the Golay- cell fixed at a distance of 150 mm. The same curve was computed by applying the Stratton-Chu formula to the electric near-field that we extract after the two-dimensional eigenfrequency-analysis. Figure 4(b) compares the two results. A very good agreement is obtained, which unambiguously demonstrates the accuracy of this modeling approach.

#106771 - $15.00 USD Received 23 Jan 2009; revised 26 Mar 2009; accepted 5 Apr 2009; published 8 Apr 2009

4. Perspectives for optimization

Beyond the accuracy, the power of this model lies in the fact that it allows the prediction of the properties of arbitrary gratings, as it does not use any assumptions on the structure except a wide waveguide and small side metallization. The only other constraint is that the metallic grating also acts as an electrical contact, so that the slits in places with electric field maxima of the mode should be relatively small, depending on the active region thickness, to avoid inhomogeneous pumping, as it was observed for instance in [19]. Within these limits, the problem we now face is to find an arbitrary digital function (metal/slit), which yields, at the highest quality factor, a coupling-efficiency well adapted to the gain properties, while maintaining a good overlap of the optical mode with the active region and a collimated vertical emission. Of course the same approach can be applied to dielectric gratings in other semiconductor lasers fabricated by optical contact lithography. As a preliminary example, we optimize our grating design in terms of radiative efficiency, which determines the differential external quantum efficiency $\eta_d=\eta_{int}\alpha_m/\alpha_{tot}$ and thus the slope efficiency. We consider the spectrum and radiative efficiency of a 42 period grating with a dc of 80 %, with two small phase-shifts of $\pi/5$ at period 7 and 35, plus a $\pi/2$ phase-shift in the center. Figure 5 shows the comparison between this and a standard grating with a dc of 80 %. The radiative efficiency of the highest quality-factor mode is increased by more than a factor of 5, while still emitting the major part of the power within ± 15 degrees with respect to the surface normal. The resonances on the high-energy side of the band-gap are not shown, because their quality factors are still strongly reduced by the very large surface losses.

Acknowledgments

This work was supported in part by the European Commission through the Research and Training Network "Physics of Intersubband Semiconductor Emitters" and the integrated project "Teranova". We acknowledge Jérôme Faist for useful discussions.

#106771 - $15.00 USD Received 23 Jan 2009; revised 26 Mar 2009; accepted 5 Apr 2009; published 8 Apr 2009